Neuron, Volume *99*

Supplemental Information

TMC1 Forms the Pore of Mechanosensory Transduction Channels in Vertebrate Inner Ear Hair Cells

Bifeng Pan, Nurunisa Akyuz, Xiao-Ping Liu, Yukako Asai, Carl Nist-Lund, Kiyoto Kurima, Bruce H. Derfler, Bence György, Walrati Limapichat, Sanket Walujkar, Lahiru N. Wimalasena, Marcos Sotomayor, David P. Corey, and Jeffrey R. Holt

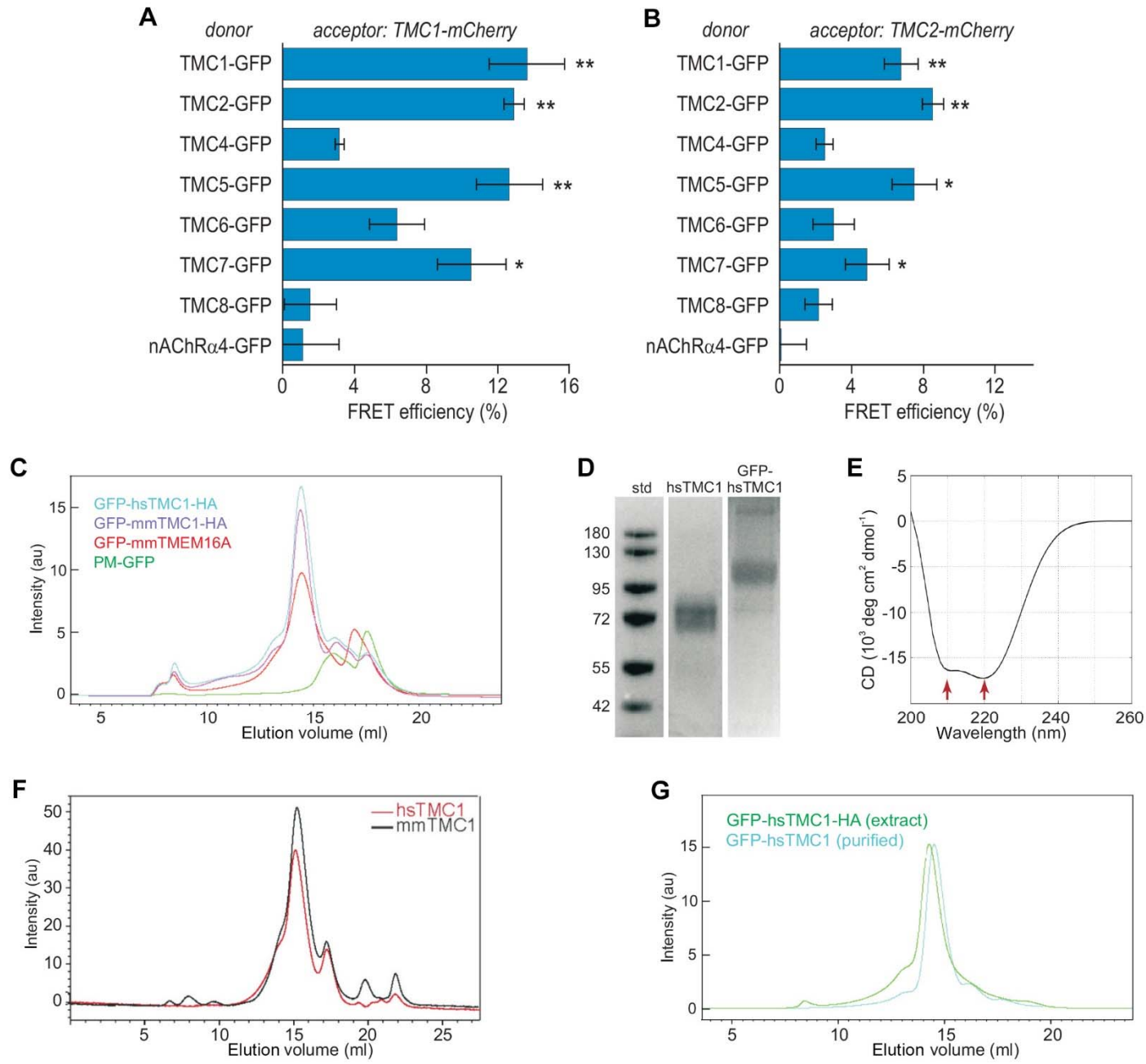

Figure S1, related to Figure 1. Biochemical Characterization of TMC1. (**A**) Fluorescence resonant energy transfer between TMC family members. mCherry at the C-terminus of TMC1 was the acceptor; GFP at the C-terminus of other TMCs was the donor. (**B**) mCherry at the C-terminus of TMC2 was the acceptor. The a4 nicotinic acetylcholine receptor served as a negative control. TMCs and nAChR were co-expressed in HEK cells. Mean ± S.D., ** $p<0.005$, * $p<0.05$. (**C**) Fluorescence Size Exclusion Chromotography (FSEC) elution profiles of GFP-hsTMC1, GFP-mmTMC1, FPmm TMEM16a and PM-GFP expressed in HEK293FT cells and extracted with resuspension buffer supplemented with 1% FOS13 (see Methods). The elution time of the protein peaks did not change when the solubilization detergent was replaced with DDM or CHS-DDM (not shown). (**D**) Coomassie stain of purified hsTMC1 proteins with and without GFP tag. (**E**) Circular dichroism assay on purified protein, indicating proper folding and high alpha-helix content. (**F**) Size-exclusion chromatography profile of purified TMC1 samples over a Superose 6 column. (**G**) FSEC profile of hsTMC1 before and after purification.

Figure S2, related to Figure 1: Mass spectrometry of purified hsTMC1. (**A**) Trypsin digestion. Peptides detected with mass spectroscopy are shown in green. Predicted TM domains (underlined in red) are not well covered, consistent with limited accessibility of trypsin for buried segments. Sites for which phosphorylation was evidenced with high certainty are boxed (modscores of 1000, 63, 1000, 60 and 80 in residue order). (**B**) Chymotrypsin digestion. Additional residues detected are shown in pink. Nearly all of the sequence was detected with mass spectroscopy, indicating synthesis and purification of full-length protein.

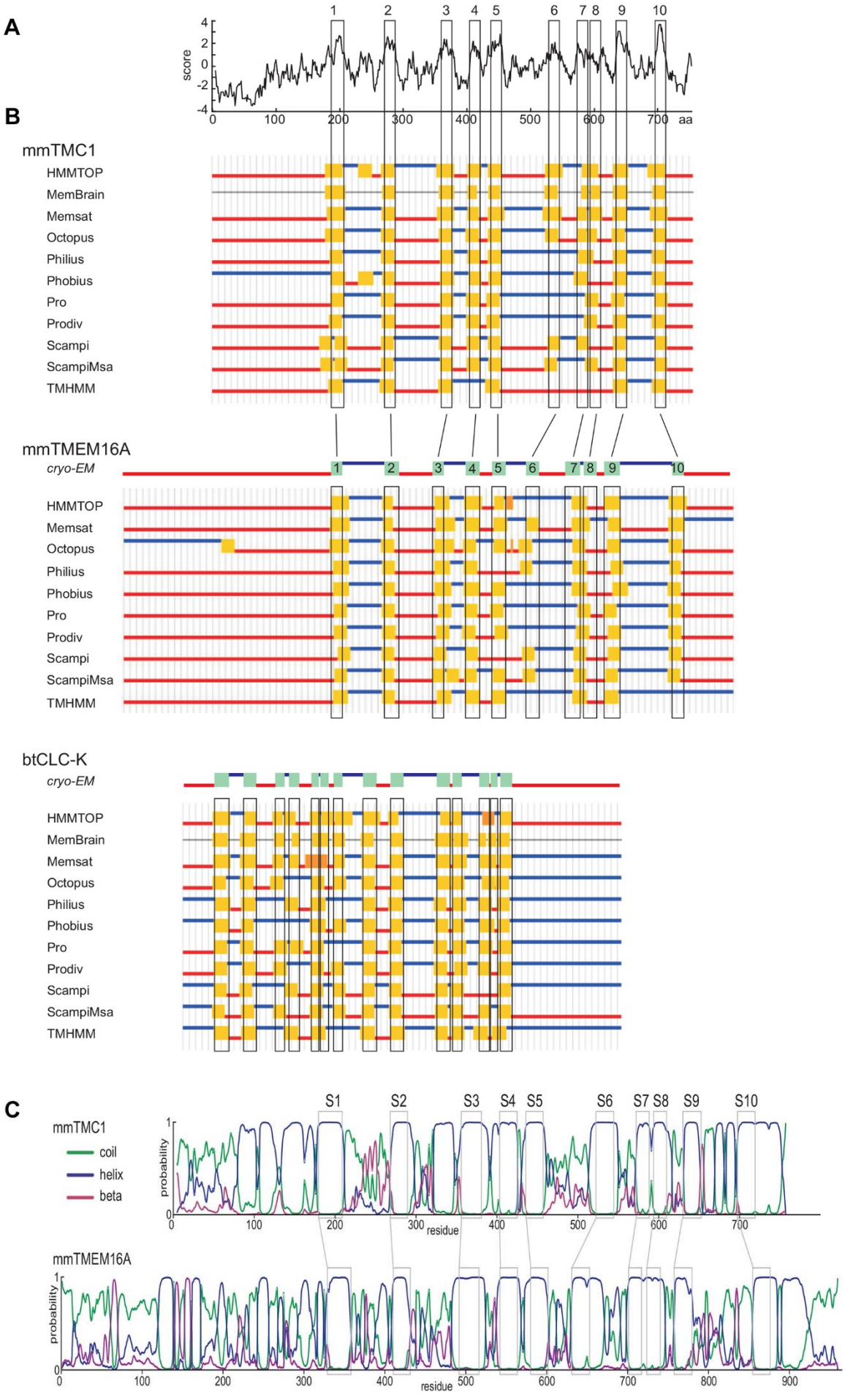
A
B
C
score
aa
mmTMC1
HMMTOP
MemBrain
Memsat
Octopus
Philius
Phobius
Pro
Prodiv
Scampi
ScampiMsa
TMHMM
mmTMEM16A
cryo-EM
btCLC-K
coil
helix
beta
probability
residue
S1
S2
S3
S4
S5
S6
S7
S8
S9
S10

Figure S3, related to Figure 1. Transmembrane domain and secondary structure predictions for TMC1, based on the structure of TMEM16A. (**A**) Hydrophobicity plot of mmTMC1 calculated by the Kyte-Doolittle method (ExPASy ProtScale). (**B**) Transmembrane domain predictions for mmTMC1 and for two representative dimeric ion channels, mmTMEM16A and btCLC-K, by the Constrained Consensus Topology (CCTOP) prediction server, which aggregates predictions from several transmembrane prediction servers. Structures of mmTMEM16A and btCLC-K have been solved by cryo-EM (Paulino et al.,2017; Park et al., 2017). Boxed regions for mTMEM16A and btCLC-K are transmembrane domains based on cryo-EM structures, indicated in cyan. No server predicted the known structures perfectly, but the prediction pattern for mmTMC1 was similar to that of mmTMEM16A and not to that of btCLC-K. Boxes for mmTMC1 indicate transmembrane domains estimated from the hydrophobicity, from CCTOP predictions, and from similarity to mmTMEM16A. (**C**) Secondary structure predictions for mmTMC1 and mmTMEM16A, generated by the Protein Secondary Structure PREDiction server (PSSpred; https://zhanglab.ccmb.med. umich.edu/PSSpred/). The probability of contributing to a coil, helix or beta strand structure is indicated for each residue. Boxed regions for mmTMEM16A based on cryo-EM structure. Boxed regions for mmTMC1 are similar in likely helical structure.

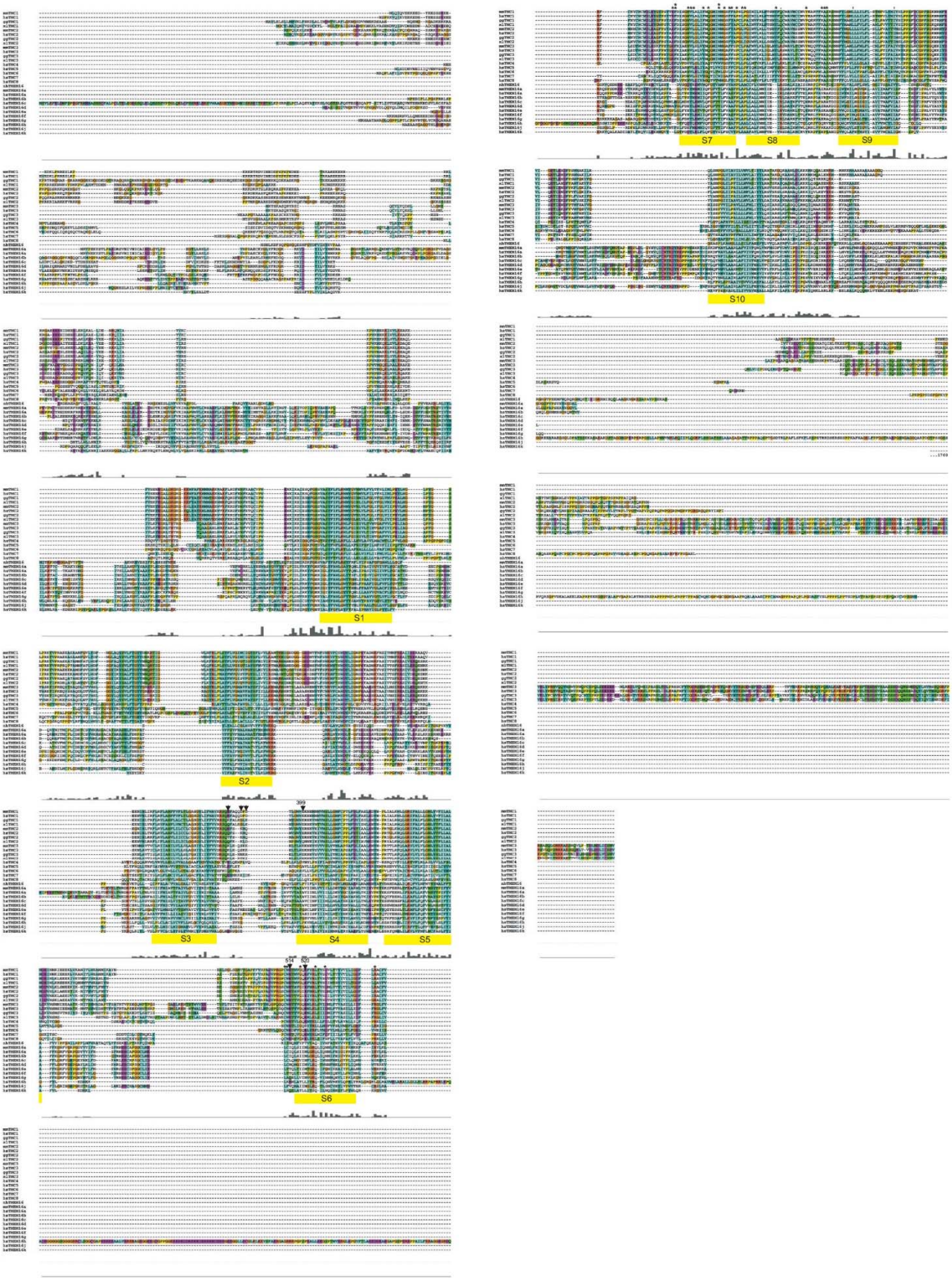

Figure S4, related to Figure 1 and Data S1. Alignment of the TMC family with the TMEM16 family. Alignment was done using ClustalX and adjusted to align secondary structure and putative transmembrane domains. The ten transmembrane domains predicted for TMCs are labeled S1-S10. See Data S1 for high resolution.

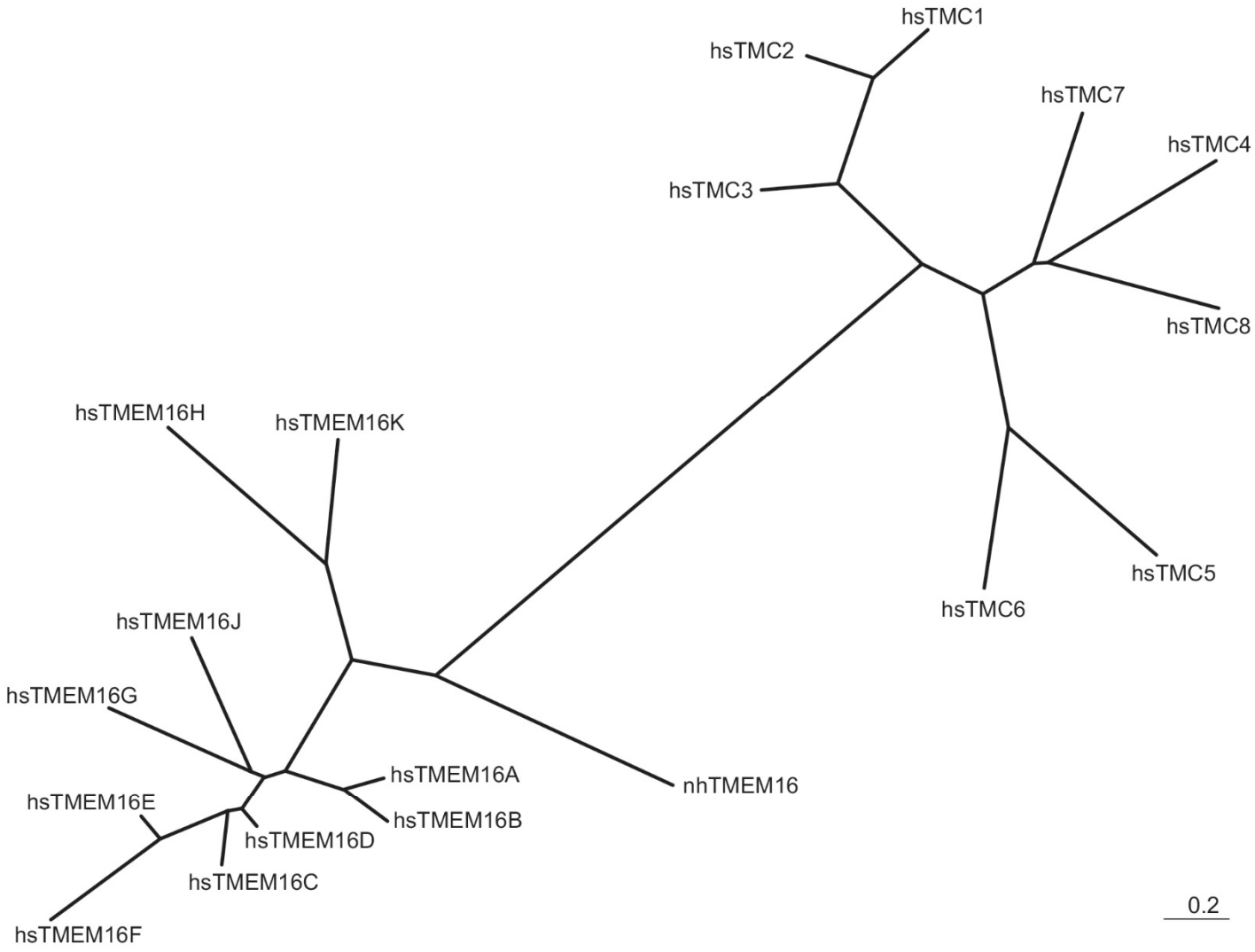

Figure S5, related to Figure 1. Phylogeny of the TMEM16 and TMC families. An unrooted phylogeny tree was produced from the alignment in Figure S4 by ClustalX2 using the neighbor-joining method, excluding positions with gaps and correcting for multiple substitutions. Only *Nectria* and human orthologs are shown here. TMCs and TMEM16s cluster into two distinct families, but the phylogenetic distance between them is not very much more than distances within them, or, for instance, between more distant members of the TRP channel family. Scale bar indicates phylogenetic distance.

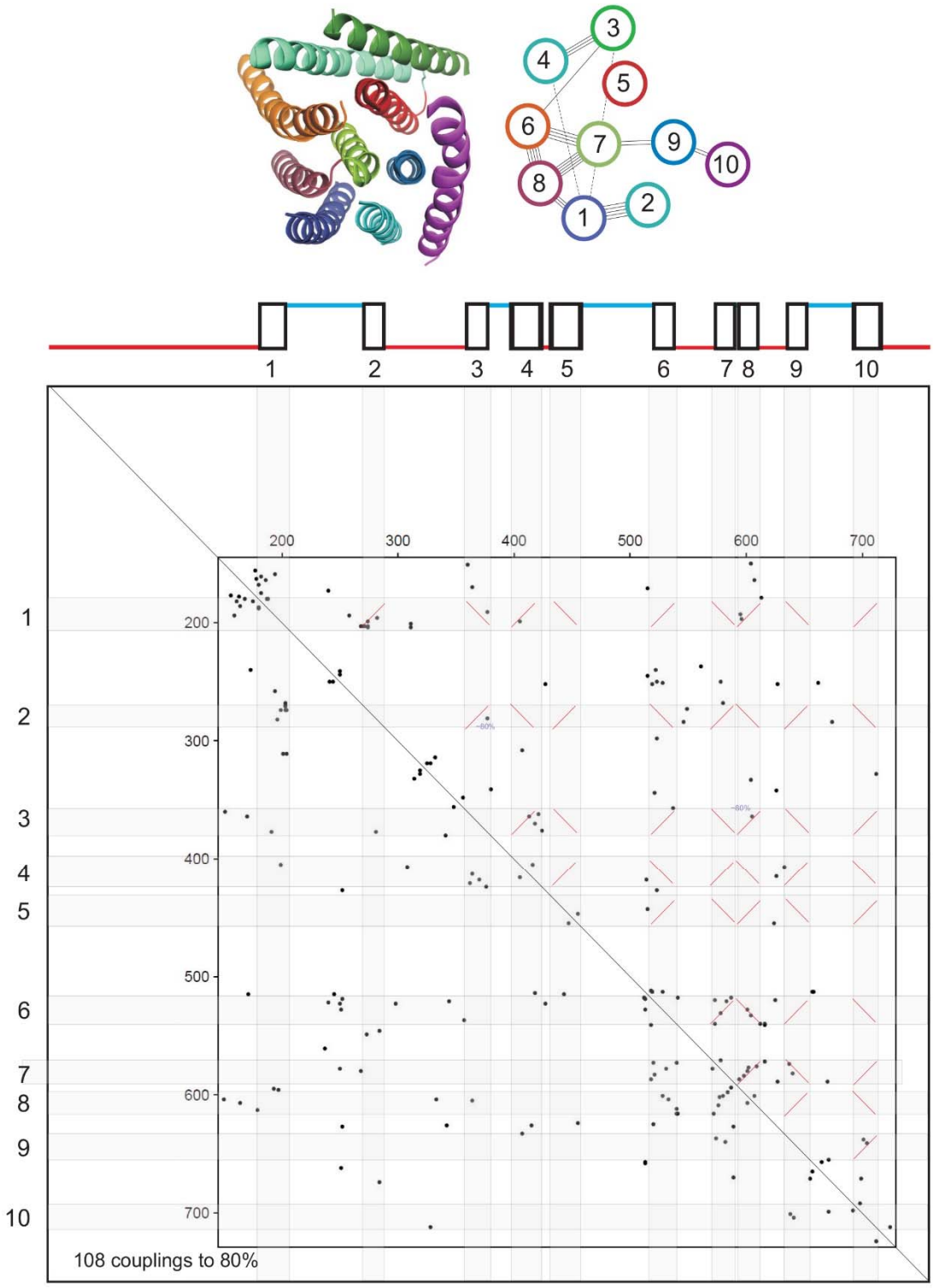

Figure S6, related to Figure 2. Evolutionary coupling among residues in mmTMC1. From an alignment of ~3500 TMC sequences, the EVcoupling algorithm identified residue pairs with high likelihood of coevolution and thus high likelihood of being adjacent in the tertiary structure. Shown are 108 couplings with >80% confidence in mouse TMC1 residues 140-735, plotted as individual dots according to sequence number, and overlaid on the predicted transmembrane domains. Oblique red lines indicate expected positions of couplings for parallel and anti-parallel helices, if the helices are adjacent. ***Top*:** the predicted transmembrane helices of one TMC1 monomer are shown as viewed from outside the cell (left) together with circles representing their relative positions (right). Couplings for residues within transmembrane domains are shown as single lines between the circles. Most couplings are between helices predicted to be adjacent.

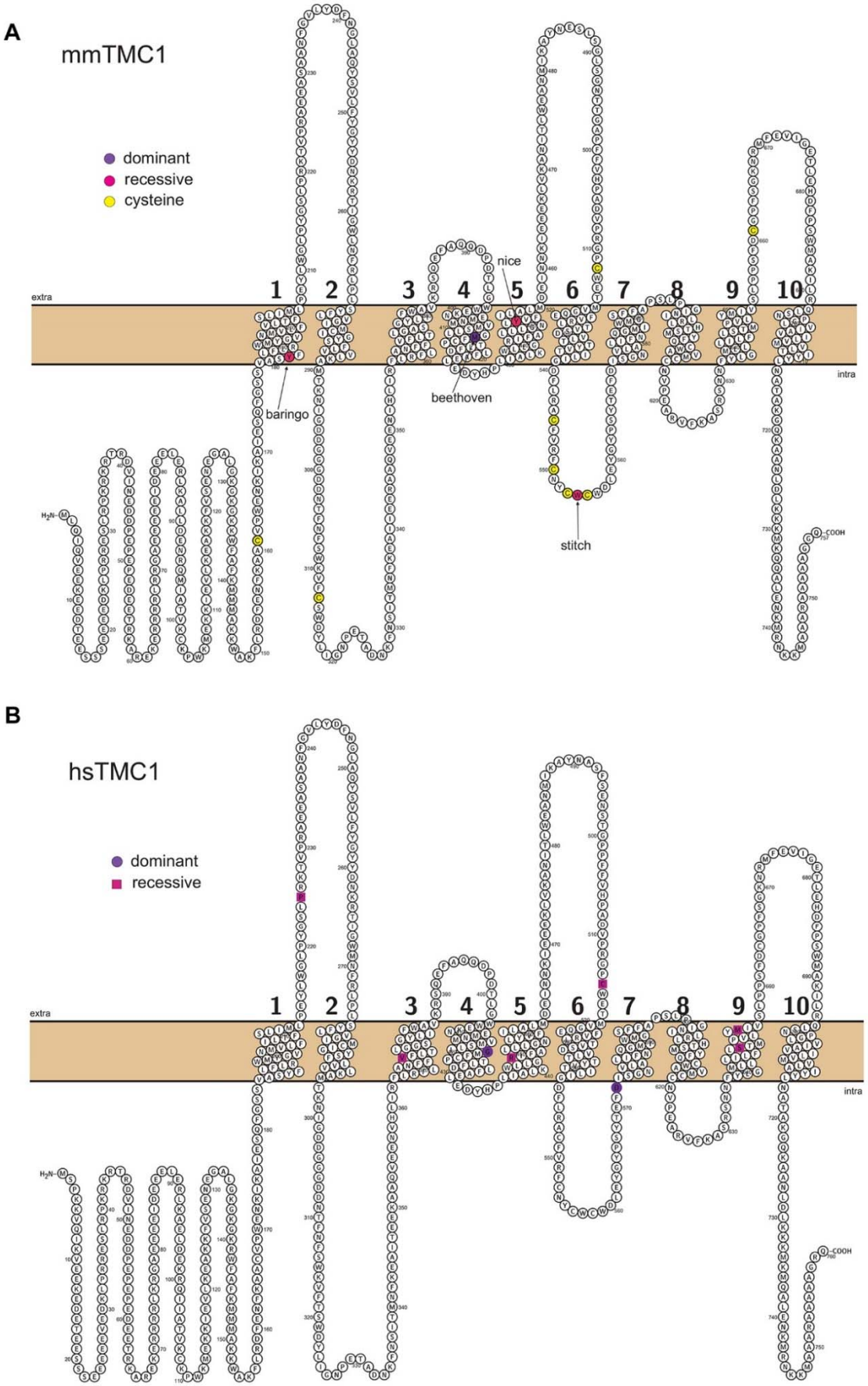

Figure S7, related to Figure 2. Proposed ten transmembrane topology for TMC1. (**A**) Missense mutations in mouse TMC1 that cause dominant or recessive deafness. Exposed cysteines are indicated in yellow. (**B**) Missense mutations in human TMC1 that cause dominant (DFNA36) or recessive (DFNB7/11) deafness.

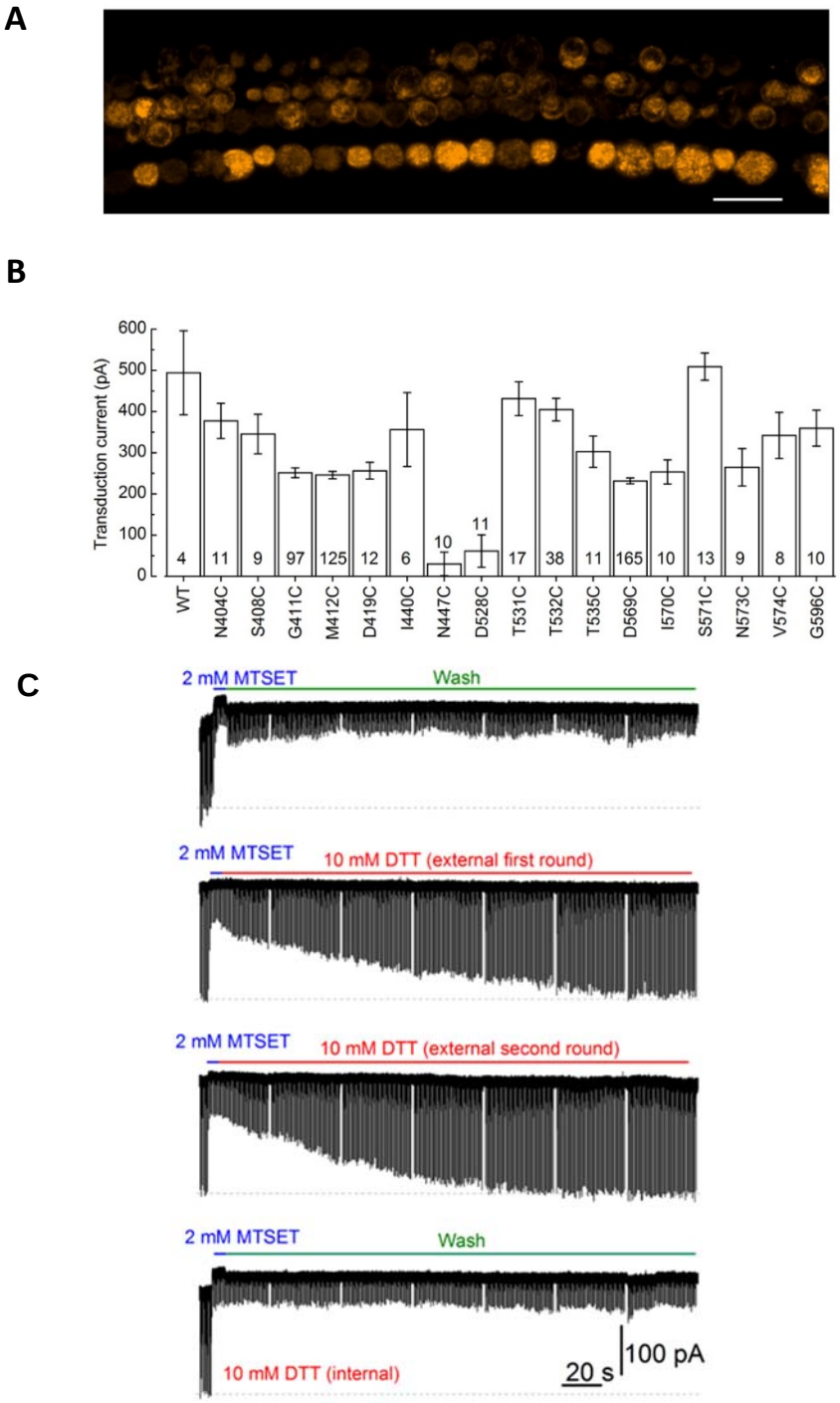

Figure S8, related to Figure 3. FM1-43 uptake in *Tmc1*$^{\Delta/\Delta}$;*Tmc2*$^{\Delta/\Delta}$ hair cells and mean sensory transduction currents. (**A**) 5 µM FM1-43 was bath applied for 10 seconds, followed by 5 minute wash in standard extracellular saline. The tissue was imaged with an FM1-43 filterset and confocal microscopy. Scale bar = 20 µm. Fluorescent cells exposed to nM concentrations FM1-43 (see *Electrophysiology* methods) were selected for recording. (**B**) Mean maximal amplitude sensory transduction currents (± SEM) recorded from cochlear inner hair cells of *Tmc1/Tmc2* mutant mice exposed to AAV2/1-*Tmc1* sequences as indicated below each bar. Number of cells, from 2 to 55 mice/substitution is shown at the bottom. (**C**) D569C current cannot be recovered by washout of MTSET, but does recover following DTT application. The top trace shows that a 10 sec application of 2 mM MTSET inhibited D569C current. After MTSET was washed out, the current did not recover even after 30 mins of wash in standard extracellular solution. The first 3 minutes of wash are shown. The two middle two

traces show responses to a 10-sec puff of 2 mM MTSET followed by bath application of 10 mM DTT, a reducing agent that breaks disulfide bonds. The D569C current was fully recovered within 2 min following DTT application, consistent with disruption of the covalent linkage between D569C and MTSET. The two middle traces were recorded from the same cell, indicating that D569C current can be repetitively inhibited by MTSET and recovered by DTT. The lower trace was obtained with external application of 2 mM MTSET, with 10 mM DTT in the internal solution. (n > 5 cells in each group from 2 mice/group).

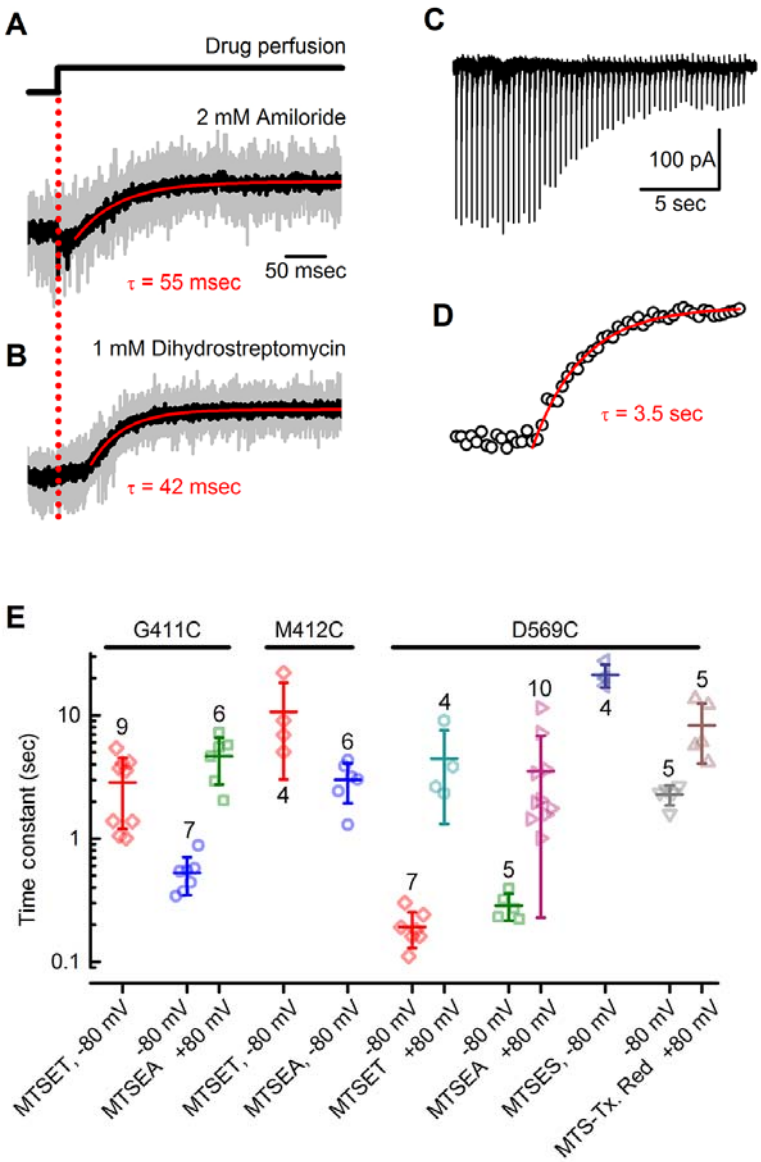

Figure S9, related to Figures 3, 5 and 6. Kinetics of MTS reactions. (A) Time course of drug perfusion system was evaluated with open-channel blockers, amiloride and DHS **(B)**, applied to six and seven IHCs, respectively. Individual traces (gray) were averaged (black) and fitted with single exponential equations (red). Application of 2 mM amiloride revealed a 34 msec perfusion delay and a 42 msec time constant (A). Application of 1 mM DHS revealed a 13 perfusion msec delay and a 55 msec time constant (B). **(C)** Representative example of the time course of G411C response to 2 mM MTSET. **(D)** Peak currents shown in panel C were extracted and plotted (open circles) and fitted with a single exponential equation that had a time constant of 3.5 sec (red line). **(E)** Mean ± S.D. time constants for G411C, M412C and D569C, for the conditions shown at the bottom. Time constants were calculated as shown in panels C, D. Number of cells from 2-5/condition is indicated.

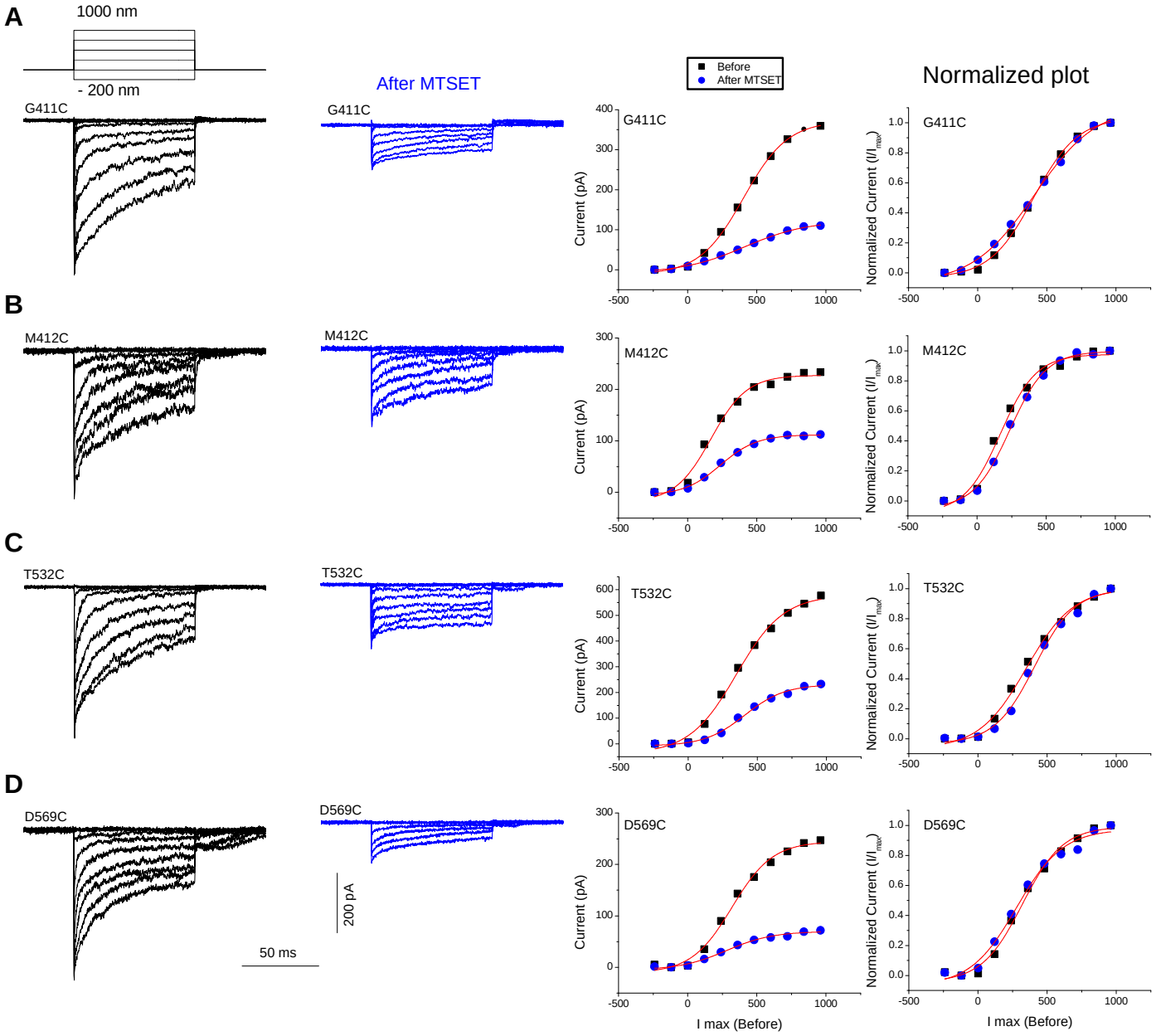

Figure S10, related to Figure 3. Representative families of current recorded from cells expressing cysteine mutants. Sensory transduction currents were recorded in response to hair bundles deflections between -200 nm to 1000 nm from IHCs expressing G411C (**A**), M412C (**B**), T532C (**C**) or D569C (**D**) before (black) and after (blue) MTSET treatment (n > 5 in each group). Stimulus-Response curves were generated by plotting peak transduction current (I) as a function of bundle displacement (X) before (black) and after (blue) MTSET, taken from the data on the left. The *I-X* curves were fitted with Boltzmann function (red) $I = Imax/\{1+exp[(X_0-X)/X_S]\}$, where Imax is maximal current, X_0 is the displacement of half activation, and X_S is the slope factor. When the data were normalized (right), the steepness of the I-X curves did not show significant difference before and after MTSET application, indicating hair bundle sensitivity was unaltered.

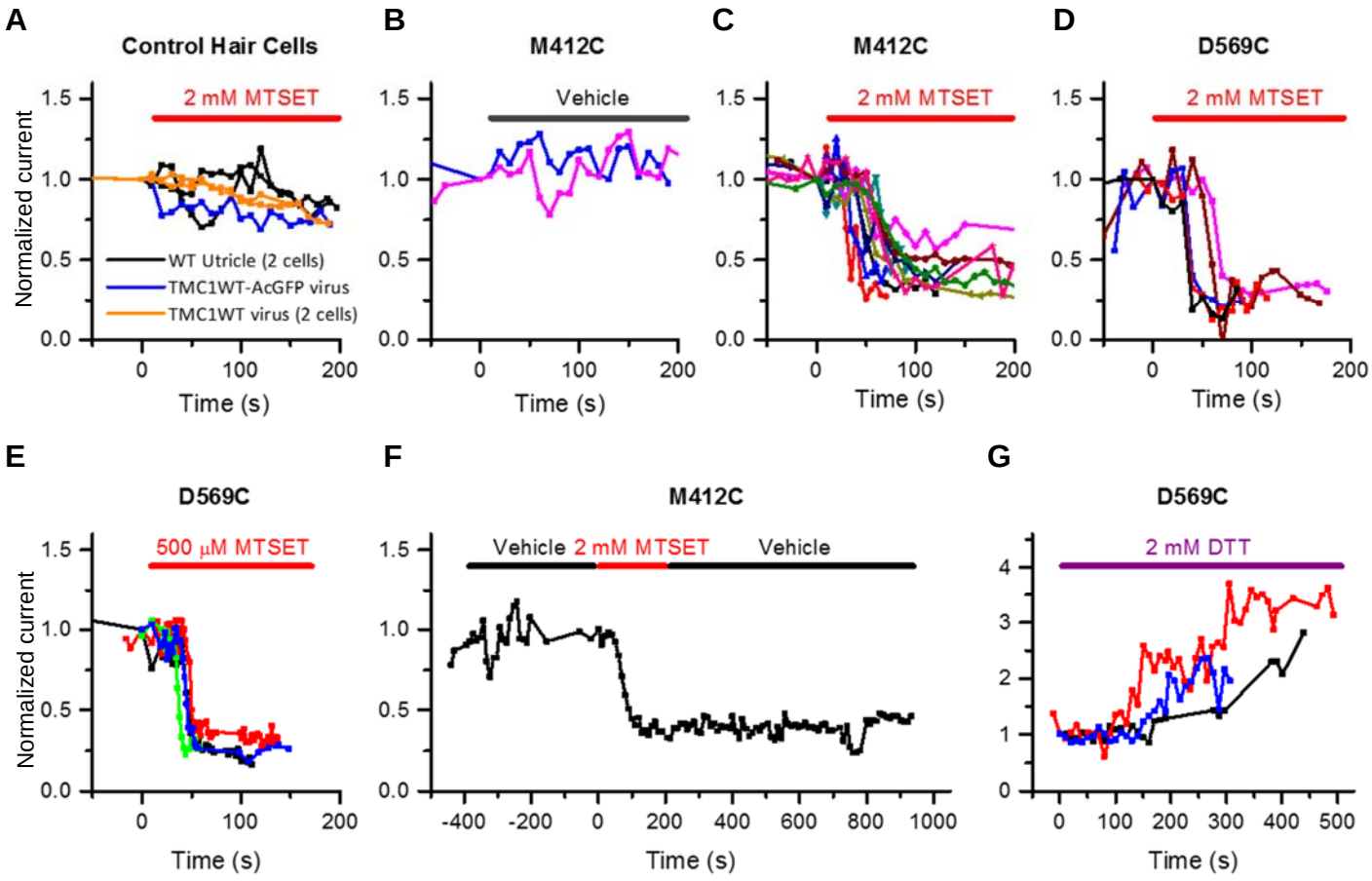

Figure S11, related to Figure 3. Sensory transduction currents recorded from M412C or D569C utricle hair cells. Relative transduction amplitudes were determined as the instantaneous current (*I*) divided by the initial current (I_0) at time 0. (**A**) Control experiments show current amplitudes from three different hair cell groups: WT utricle hair cells (black), *Tmc1/Tmc2*-null cells expressing TMC1 WT-AcGFP (blue) and TMC1-WT (orange) during application of 2 mM MTSET. (**B**) Two examples of M412C currents that demonstrate no decline current amplitude during a 200 sec application of standard extracellular solution. (**C**) Relative current amplitudes for nine M412C cells in response to 2 mM MTSET revealed ~60% decline in current amplitude. (**D,E**) Responses of five D569 utricle cells exposed to 2 mM (**D**) or 0.5 mM (**E**) MTSET. (**F**) Application of 2 mM MTSET resulted in an irreversible decay in M412C current following 800 sec wash. (**G**) Following MTSET exposure at time 0, the D569C current slowly recovered in response to 2 mM DTT application.

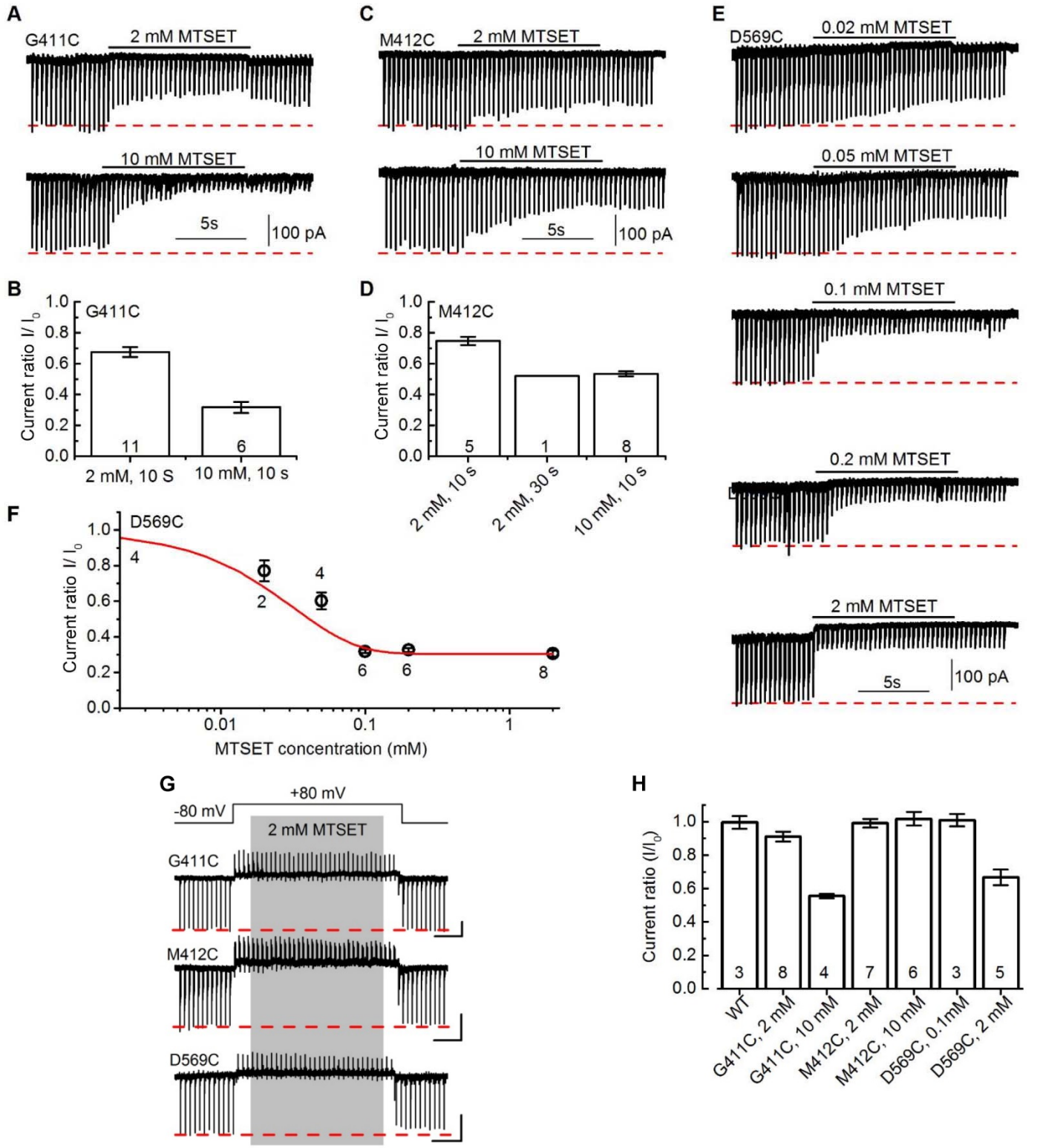

Figure S12, related to Figure 3. MTSET inhibition of sensory transduction current in G411C, M412C, and D569C IHCs. (**A**) Representative current traces showed that G411C current inhibition was faster and to a great extent with a 10-sec application of 10 mM MTSET (bottom) than 2 mM MTSET (top). (**B**) G411C mean (±SEM) current ratios (I/I_0) demonstrated that ~35% block at 2 mM (black) vs 70% block at 10 mM (red). (**C**) Representative traces for M412C IHCs in response to 2 mM MTSET (top) and 10 mM MTSET (bottom). (**D**) Mean (±SEM) current ratios (I/I_0) for M412C IHCs. (**E**) Current traces from D569C cells exposed to MTSET concentrations between 20 µM and 2 mM. (**F**) Current ratios (I/I_0) induced after a 10 s application of MTSET at concentrations that ranged

from 20 µM to 2 mM. Data were fit with an exponential equation that had a half blocking concentration of ~0.05 mM. Number of cells, from 1 to 3 mice, are indicated for each concentration. (**G**) Three substitutions, G411C, M412C, and D569C were examined for voltage-dependence of the MTSET reaction by depolarizing from the holding potential of −80 mV to +80 mV (top trace) while stimulating the bundle. Red line indicates mean current level prior to MTSET application. Scale bars indicate 2 seconds (horizontal) and 100 pA (vertical) for each trace. (**H**) Mean current ratios (±SEM) measured as the mean from the first 5 steps and the last 5 steps plotted for WT and three cysteine substitutions each at two different MTSET concentrations. Number of cells, from 1 to 3 mice, is shown at the bottom of each bar.

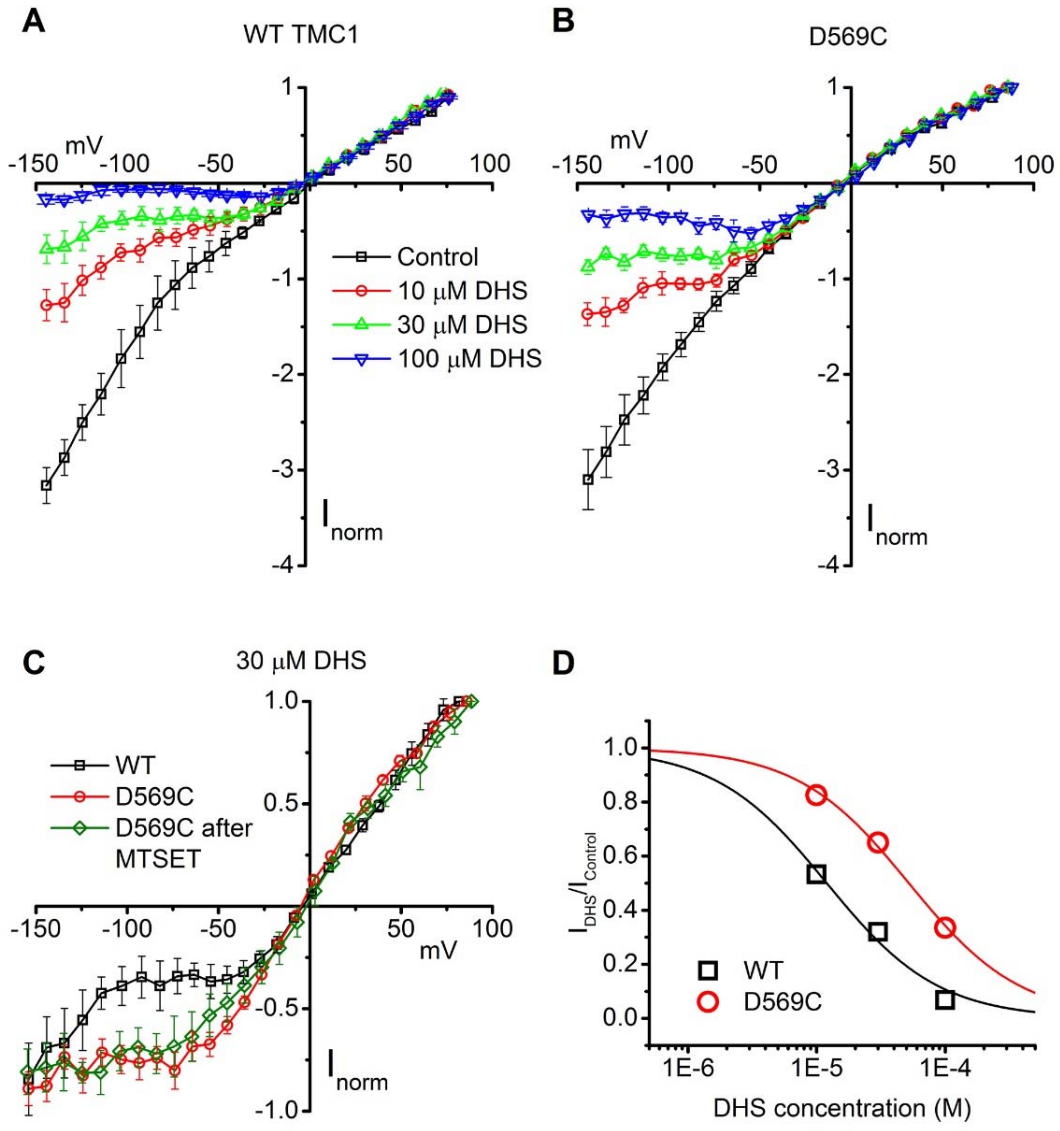

Figure S13, related to Figure 7. D569C mutation alters the affinity for extracellular DHS. (A) Mean current-voltage relationships in utricle type II hair cells expressing WT TMC1. Currents were measured in control solutions and extracellular DHS applied at three concentrations (control, n = 3; 10 µM, n = 4, 30 µM, n = 3; 100 µM, n = 3, 2 mice/concentration). Current amplitudes were normalized to the current at nominal +100 mV. DHS produced a block at negative potentials that was partially relieved at very negative potentials (<-100 mV), as previously described and interpreted as passage of DHS through the channel at large negative voltages (Marcotti

et al., 2005; Corns et al., 2016). **(B)** Mean current-voltage relations in cells expressing D569C exposed to various concentrations of DHS (control, n = 6; 10 µM, n = 6; 30 µM, n = 6; 100 µM, n = 4, 2-3 mice/concentration). **(C)** Mean current-voltage relations from panels A and B. In 30 µM DHS the curves show a reduction in block at intermediate voltages (between -25 mV and -125 mV). Application of 2 mM MTSET did not further alter the voltage-dependence of transduction current in 30 µM DHS (n = 4). **(D)** Dose-response data (symbols), extracted from panels A and B (at -76 mV). Data were fitted with the follow equation:

$$\frac{I_{DHS}}{I_{control}} = \frac{1}{1 + \frac{[DHS]}{K_d}}$$

where I_{DHS} is current measured in the presence of DHS, $I_{control}$ is the control current, [*DHS*] is the extra-cellular concentration of DHS and K_d is the half-blocking concentration (lines). The fits revealed a K_d of 12 µM for WT TMC1 (black squares), consistent with Corns et al. (2016; 14 µM at −81 mV) and 52 µM for D569C.

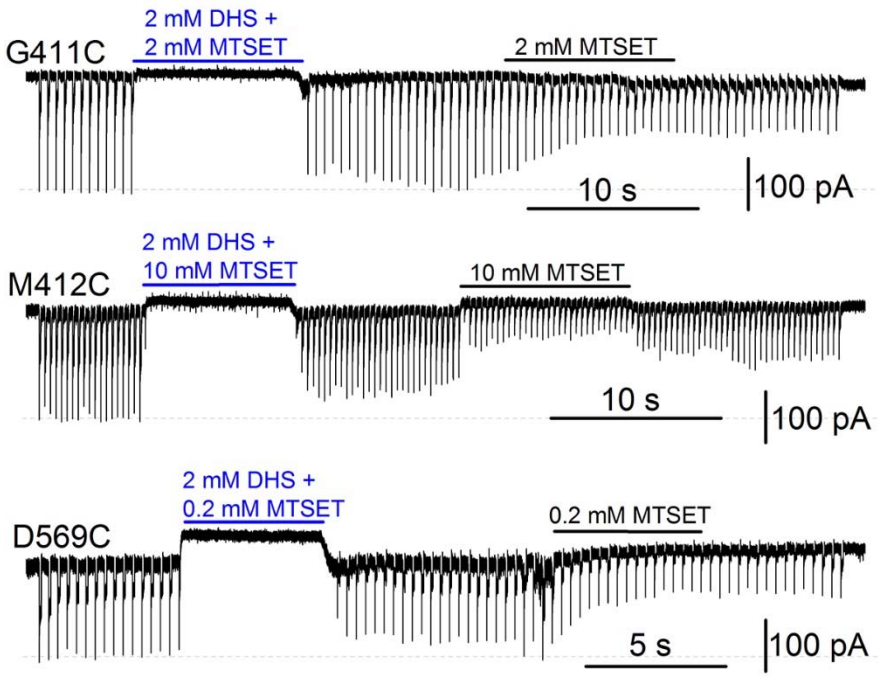

Figure S14, related to Figure 7. DHS protected transduction channels from MTSET reagents. IHCs expressing G411C (top), M412C (middle), or D569C (bottom) mutations were exposed to 2 mM DHS and MTSET at the concentrations indicated. Following washout, MTSET alone was reapplied, revealing an irreversible decline in current amplitude ($n > 5$ for each group). The data demonstrate that DHS protected the channels from reacting with MTSET and that the cysteine sites were still available to react with MTSET alone.

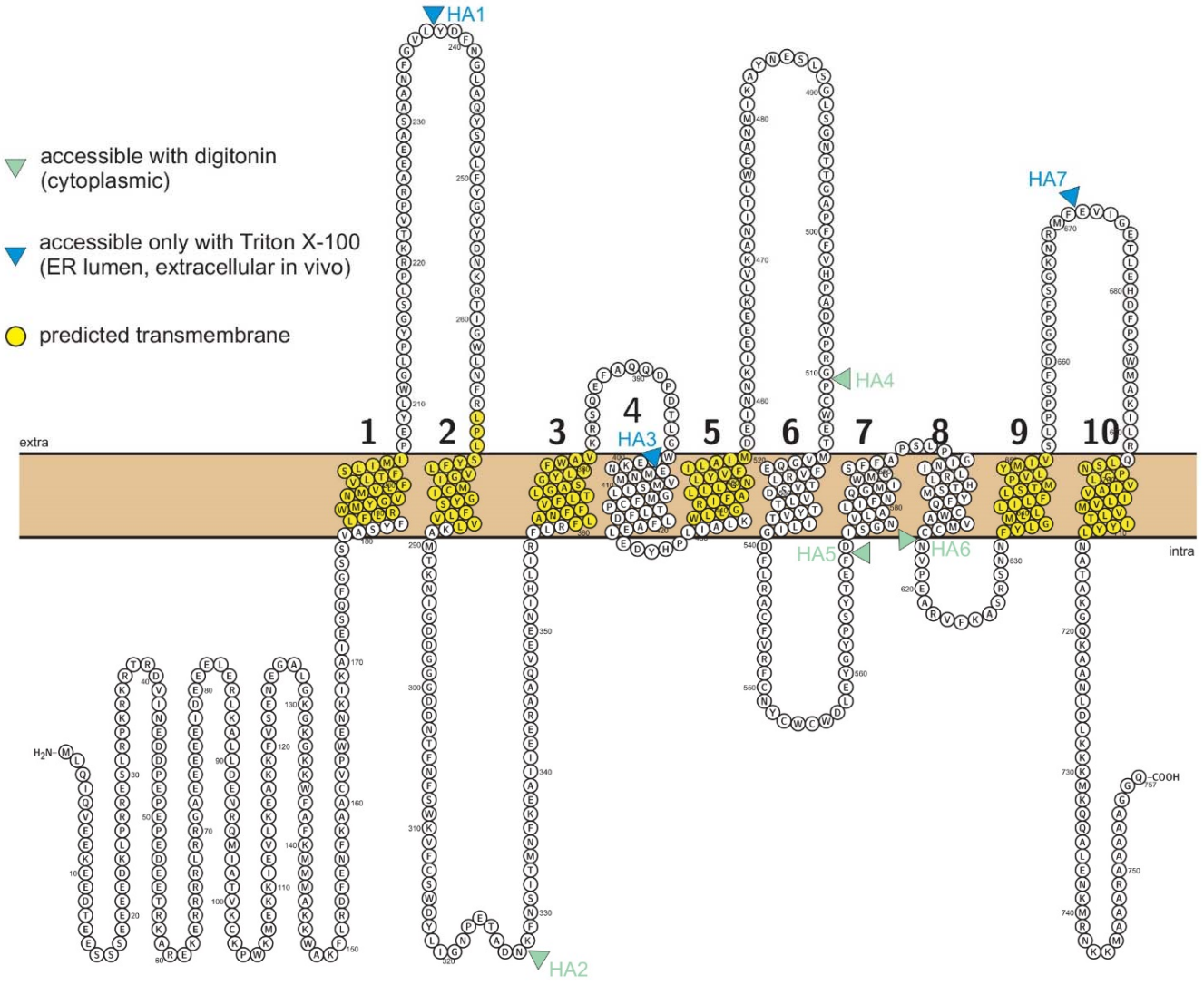

Figure S15, related to Figure 2. Comparison of predicted topology to Labay et al., (2010). Labay et al. inserted hemaggutinin tags (HA tags; triangles) into seven sites in mouse TMC1 and tested accessibility of the tags to anti-HA antibodies. Because mmTMC1 was retained in the endoplasmic reticulum, they used a differential treatment with detergents that allowed (Triton X-100) or did not allow (digitonin) access to the ER lumen (corresponding to the extracellular side when TMC1 is in the plasma membrane). Tags HA1, 3 and 7 were not accessible if only digitonin was used suggesting these are extracellular. They predicted a topology with six transmembrane domains (yellow), based on the accessibility experiments and a transmembrane domain analysis by TMHHH2.0. Our ten transmembrane topology includes the six domains predicted by Labay et al. plus four additional domains (S4, S6, S7 and S8). Our revised topology is consistent with the intracellular / extracellular accessibility of six of the Labay et al. HA tags. We suggest the region surrounding HA4 is extracellular.